DC FIELD EMISSION SCANNING MEASUREMENTS ON ELECTROPOLISHED NIOBIUM SAMPLES

Arti Dangwal[1,2,#], Detlef Reschke[2], Günter Müller[1]

[1] FB C Physik, Berg. Universität Wuppertal, Gaußstraße 20, D-42097 Wuppertal, Germany

[2] DESY, D-22603 Hamburg, Germany

Abstract

Electropolished (EP) Nb samples were investigated by a dc field emission scanning microscope, which has recently been modernized for the fast scans on large samples. Measurements on EP samples before and after high pressure rinsing (HPR) are compared. Reproducible voltage scans at various surface fields have been obtained partially down to μm resolution. The statistical overview of the density of emitting sites at 120 MV/m shows a reduction from about 30 before to 14 emitters/cm^2 after HPR. Local measurements of selected emitters prove increased onset fields E_{on} at 1 nA and decreased β values after HPR. High resolution SEM images and EDX measurements of the identified emitters will also be presented.

Keywords: Field emission, scanning microscope, electropolishing, Niobium, high pressure rinsing.

1. INTRODUCTION

Enhanced field emission (EFE) from particulates and surface irregularities is one major obstacle which has to be overcome for efficient high gradient operation of superconducting niobium cavities. Accelerating gradients up to 30 (40) MV/m, corresponding to peak electric surface fields of about 60 (80) MV/m at the cavity irises, are envisaged for accelerators like the X-ray free electron laser (XFEL) approved at DESY [1] and the international linear collider (ILC) under design now [2], respectively.

In order to avoid EFE in these cavities reliably, typical field emitters on Nb surfaces resulting from the actually used surface preparation techniques must be identified. Since electropolished (EP) Nb surfaces are considered to improve the achievable cavity fields, we have started to investigate large area EP Nb samples by means of the dc field emission scanning microscope (FESM) [3]. This apparatus has recently been modernized with new hardware components (Keithley picoamperemeter with 1 kHz rate, FUG power supply with PID regulation) [4] and LabVIEW based programs, resulting in fast voltage scans of large samples thus improving the statistics of the FESM measurements.

First results of voltage scans up to 120 MV/m with a successive change of resolution by anode tip diameters ranging from 300 μm to 2 μm and local measurements are presented. The density of emitting sites, onset field E_{on} at 1 nA and β values of localized emitters will be compared on a EP Nb sample before and after high pressure rinsing

_____
#arti@physik.uni-wuppertal.de

(HPR). High resolution SEM images and EDX analysis of selected emitting sites will also be presented.

2. EXPERIMENTAL

Two Nb samples of 28 mm diameter previously tested after buffered chemical polishing [5] were electropolished (140 μm) and clean water rinsed at CEA Saclay. Contamination of these samples was avoided by cleanroom assembly and a special transport system which has been opened inside the load lock of the field emission scanning microscope (FESM) at 10^{-6} mbar. For comparison, one sample (SEP2) was cleaned in a new HPR facility at DESY with similar parameters as used for cavities, i.e. at a pump pressure of 150 bar, a rotation speed of 4-5 rpm and a vertical speed of 10 mm/min.

FE measurements were performed under ultra high vacuum conditions ($< 10^{-9}$ mbar). The sample stage is movable in xyz directions by computer controlled motors with about 70 nm step width or by piezo translators with nm resolution. The electrode spacing, d, is controlled by a long distance optical microscope with CCD video camera and varies less than 1 μm for well-tilted flat samples [3]. Emitter distributions were obtained by the voltage scans, V(x, y), with a constant PID-regulated current of 1 nA, the spatial resolution of which is limited by the selected W anode and electrode spacing. Five different anodes (tip diameters $\varnothing_{Anode}$ = 2 to 300 μm) were used for the complete series of measurements. The resulting typical measurement time for one map of 100×100 pixels is about 1 h. At pronounced emitting sites, appropriate subroutines provide V(z) plots at constant current (1 nA) for distance and field calibration and I-V curves for Fowler-Nordheim (FN) analysis. Finally in-situ SEM images with moderate spatial resolution (~ 1 μm) are taken as a guide for the relocalization of emitters in the high resolution SEM (nm) with EDX analysis. A more detailed description of the measurement techniques is given elsewhere [4].

3. RESULTS AND DISCUSSION

At first both EP Nb samples were investigated in the FESM by regulated voltage scans up to 120 MV/m. Sample SEP1 showed the onset of FE at 60 MV/m and about 11 emitters/cm^2 at 90 MV/m, which were clustered in a small part of the sample (0.25 cm^2), while for most of the surface no FE occurred up to 120 MV/m. The emitter distributions measured for sample SEP2 before and after HPR are shown in Fig. 1. It should be noted that the low resolution scan series (1st series before and 3rd series after HPR) were made in the same surface area of the sample,

while the zoomed-in area of the 2nd and 4th series were slightly different according to the location of emitters.

(a) E = 40 MV/m, 1 emitter   (b) E = 60 MV/m, 3 emitters   (c) E = 90 MV/m, 6 emitters

1st Series: $\varnothing_{Anode}$ = 300 μm, d = 50 μm (± 5 μm), A = (12×12) mm^2

(d) E = 90 MV/m, 11 emitters   (e) E =120 MV/m, 0 emitter   (f) E =120 MV/m, 17 emitters
A = (12×12) mm^2 A = (5×5) mm^2 A = (7.5×7.5) mm^2

2nd Series: $\varnothing_{Anode}$ = 100 μm, d= 40 μm (± 5 μm)

(g) E = 40 MV/m, 0 emitter   (h) E = 60 MV/m, 2 emitters   (i) E = 90 MV/m, 3 emitters

3rd Series: $\varnothing_{Anode}$ = 300 μm, d = 50 μm (± 5 μm), A = (12×12) mm^2

E (MV/m)
25   40   60   90   120

(k) E = 90 MV/m, 3 emitters   (l) E = 120 MV/m, 8 emitters

4th Series: $\varnothing_{Anode}$ = 100 μm, d = 40 μm (± 5 μm), A = (7.5×7.5) mm^2

Fig. 1: Voltage maps of the same EP Nb sample before (a-f) and after HPR (g-l) taken at different field levels and showing the onset field of emitters (see color bar). The maps in (e, f, k, l) correspond to the marked areas in (d, i) respectively.

In general, most of the emitters in Figs. 1(a-f) and 1(g-l) are reproducible for increasing field level as well as for zooming into higher resolution, but some emitters become activated or better resolved then. As expected, sample SEP2 provides similar FE performance in terms of onset field and number density of emitters as sample SEP1 before HPR but improved values after HPR. Comparing Figs. 1(d) and 1(i) in detail, most of the emitters at 90 MV/m have been removed by HPR. In Fig. 1(f) and 1(l) at 120 MV/m, however, many weak emitters occur before as well as after HPR. The number density of emitters N resulting from the maps for different resolution and electric field E is given in table 1. The comparison of these N(E) data in Fig. 2 clearly proves the benefit of HPR against FE.

Table.1: Number density of emitters for various anode diameters and electric fields extracted from Fig. 1.

Φ_{Anode}	E	N (# /cm^2)	
(μm)	(MV/m)	EP only	EP + HPR
300	40	0.7	0
300	60	2.1	1.4
300	90	4.2	2.1
100	90	7.6	5.3
100	120	30.2	14.2
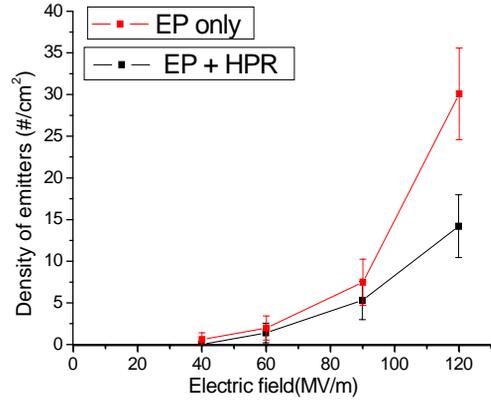
Fig. 2: Reduction of FE for SEP2 by HPR

In order to learn more about the nature of the emitters, high resolution voltage scans were performed in the most interesting area (Fig. 1(f)) of sample SEP2 before HPR. In high resolution scans, the effective electric field between the electrodes in tip-plane configuration is V/($\alpha \cdot$d), where α is a geometric correction factor which depends on the tip geometry and electrode spacing [6]. Fig. 3(a) shows more emitters than the corresponding area in Fig. 1(d), thus demonstrating the activation of emitters by high fields. The strongest emission site there splits into three FE sites for 10 μm resolution (Fig. 3(b)), which are further resolved in (Fig. 3(c)), where the resolution limit set by the actual surface roughness is reached.

(a) E = 80 MV/m, A= 6×6 mm^2 (b) E = 83 MV/m, A= 1×1 mm^2

(c) E= 85 MV/m, Δz = 12 μm, α = 4 for emitters 1(a) and (c), Δz = 10 μm, α = 3.5 for emitter 1(b)
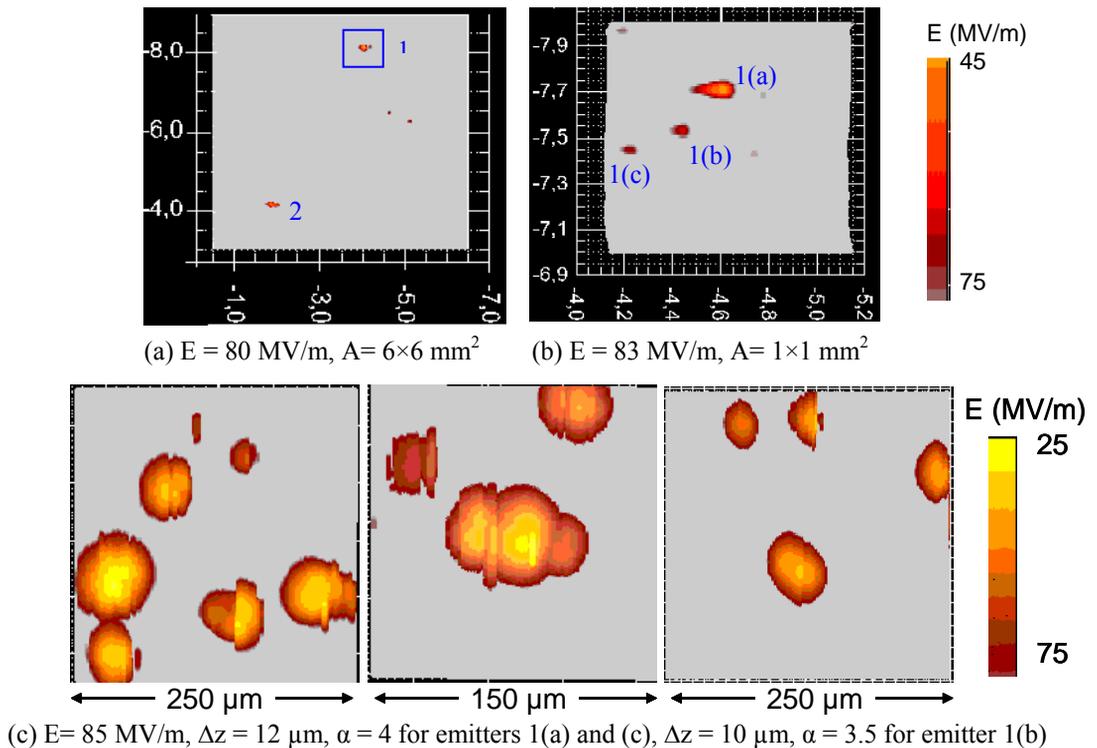
Fig 3: Zooming into emitters of sample SEP2 before HPR by high resolution maps with reduced anode diameter of (a) 30 μm, marked square resolved in (b) 10 μm and emitters #1(a-c) resolved in (c) 2 μm.

#1(a) E_{on} (1nA) = 33 MV/m
$\beta_\uparrow$ = 231, S_1 = 3.23 × 10^{-19} m^2
$\beta_\downarrow$ = 160, S_2 = 2.15 × 10^{-17} m^2

#1(b) E_{on} (1nA) = 35 MV/m
$\beta_\uparrow$ = 133.5, S_1 = 3.7 × 10^{-18} m^2
$\beta_\downarrow$ = 134, S_2 = 3.9 × 10^{-18} m^2

#1(c) E_{on} (1nA) = 45.5 MV/m
$\beta_\uparrow$ = 31.6, S_1 = 9 × 10^{-13} m^2
$\beta_\downarrow$ = 31.85, S_2 = 7 × 10^{-13} m^2

#1*. E_{on} (1 nA) = 68.7 MV/m
$\beta_\uparrow$ = 75.1, S_1 = 1.6 × 10^{-15} m^2
$\beta_\downarrow$ = 64.6, S_2 = 2.4 × 10^{-13} m^2

#3*. E_{on} (1 nA) = 48.5 MV/m
$\beta_\uparrow$ = 166.6, S_1 = 1.6 × 10^{-20} m^2
$\beta_\downarrow$ = 147.6, S_2 = 7.2 × 10^{-20} m^2

#4. E_{on} (1 nA) = 76.9 MV/m
$\beta_\uparrow$ = 19.3, S_1 = 1 × 10^{-13} m^2
$\beta_\downarrow$ = 17.9, S_2 = 5 × 10^{-13} m^2
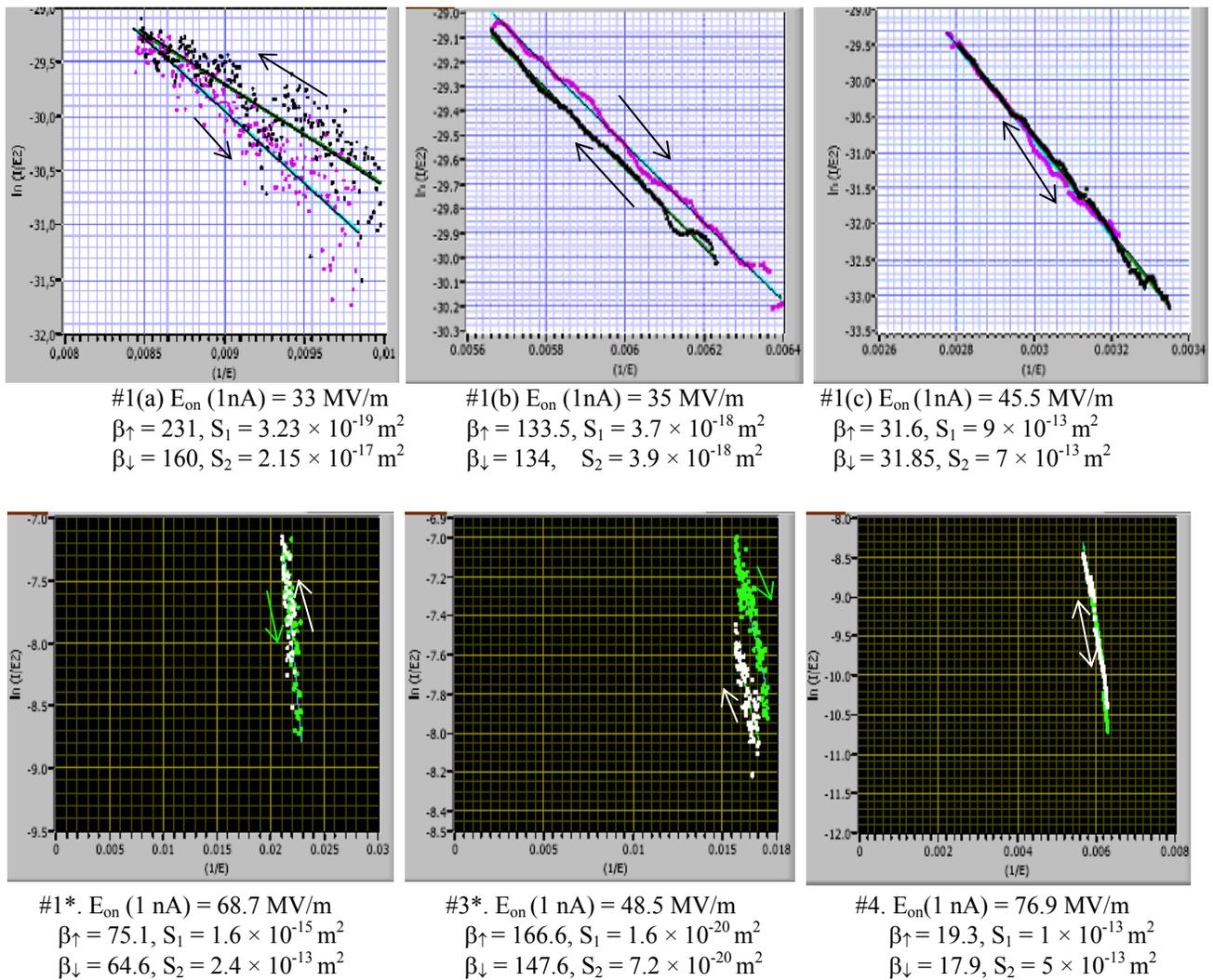
Fig. 4: FN curves of single emitters #1(a), 1(b) and 1(c) as marked in Fig. 3(b) and # 1, 3 and 4 as marked in Fig. 1(l).

Some of the emitters localized in Figs. 3(b) and 1(l) were chosen for stability and FN analysis as shown in Fig. 4. With exemption of the rather unstable emitter #1(a), all emitters clearly showed stable metallic FN behaviour partially with slight activation (e.g. #1(b) and #3*) or deactivation (e.g. #1*) effects which are well known as switch-on/off due to unstable microstructures and surface influences [7]. Obviously the emitters on this EP Nb sample were stronger before than after HPR, i.e. the onset fields E_{on}(1 nA) changed from 33-46 MV/m to 48-77 MV/m. The field enhancement factors β resulting from the slopes (for a work function Φ of 4 eV) vary less systematically between 31 and 231 and are balanced by the values of effective emission area, S, lying in the range of 10^{-20} and 10^{-12} m^2. These values are typical for EFE of Nb surfaces and can be explained by the projection model of irregular shaped particulates of μm size [8] and resonant tunnelling through electronic surface states [6].

It should be noted that only one emitter on SEP2 (#2) has survived the HPR cleaning process but weakened as shown in Figs. 5(a-b). Initially this emitter on the EP Nb sample with an E_{on}(1 nA) of 45 MV/m switches from a low β/high S into a high β/low S state, the latter being much less emissive at fields around 50 MV/m (Fig. 5(a)). After HPR this emitter (#2*) shows more stable emission in the field range 54 to 75 MV/m with as low β values as in the initial state but S parameters comparable to the final state before HPR. This puzzle might be clarified by the high resolution SEM images of this emitter in Figs. 5(c-e). Obviously a thin object of about 100 μm^2 size with a folded edge extension and sharp protrusions covers the Nb surface, which seems to be conductive according to the dark colour in SEM. Most of this object is semi-transparent for the electron beam, and the grain structure is hardly influenced. At higher magnification submicron protrusions and a rolled edge of the extension become evident. Since no foreign element (Z > 10) was detected by EDX analysis, this object might reflect a different Nb oxide state compared to the regular surface as observed in star bursts [9]. It is tempting to attribute the change of FE parameters to the alignment of protrusions with electric field and dulling of sharp edges by HPR, but further FESM investigations with submicron resolution are required to prove any of such correlations.

(a)　　$E_{on}(1\,nA) = 44.6$ MV/m
　　　$\beta\uparrow = 59.5$,　$S_1 = 8.2\times10^{-10}$ m^2
　　　$\beta\downarrow = 119$,　$S_2 = 1.2\times10^{-16}$ m^2

(b)　　$E_{on}(1\,nA) = 54.3$ MV/m
　　　$\beta\uparrow = 67.4$,　$S_1 = 2\times10^{-17}$ m^2
　　　$\beta\downarrow = 51.2$,　$S_2 = 1.2\times10^{-15}$ m^2

(c) Emitter #2　　　　(d) Emitter #2*　　　　(e) marked edge of # 2*
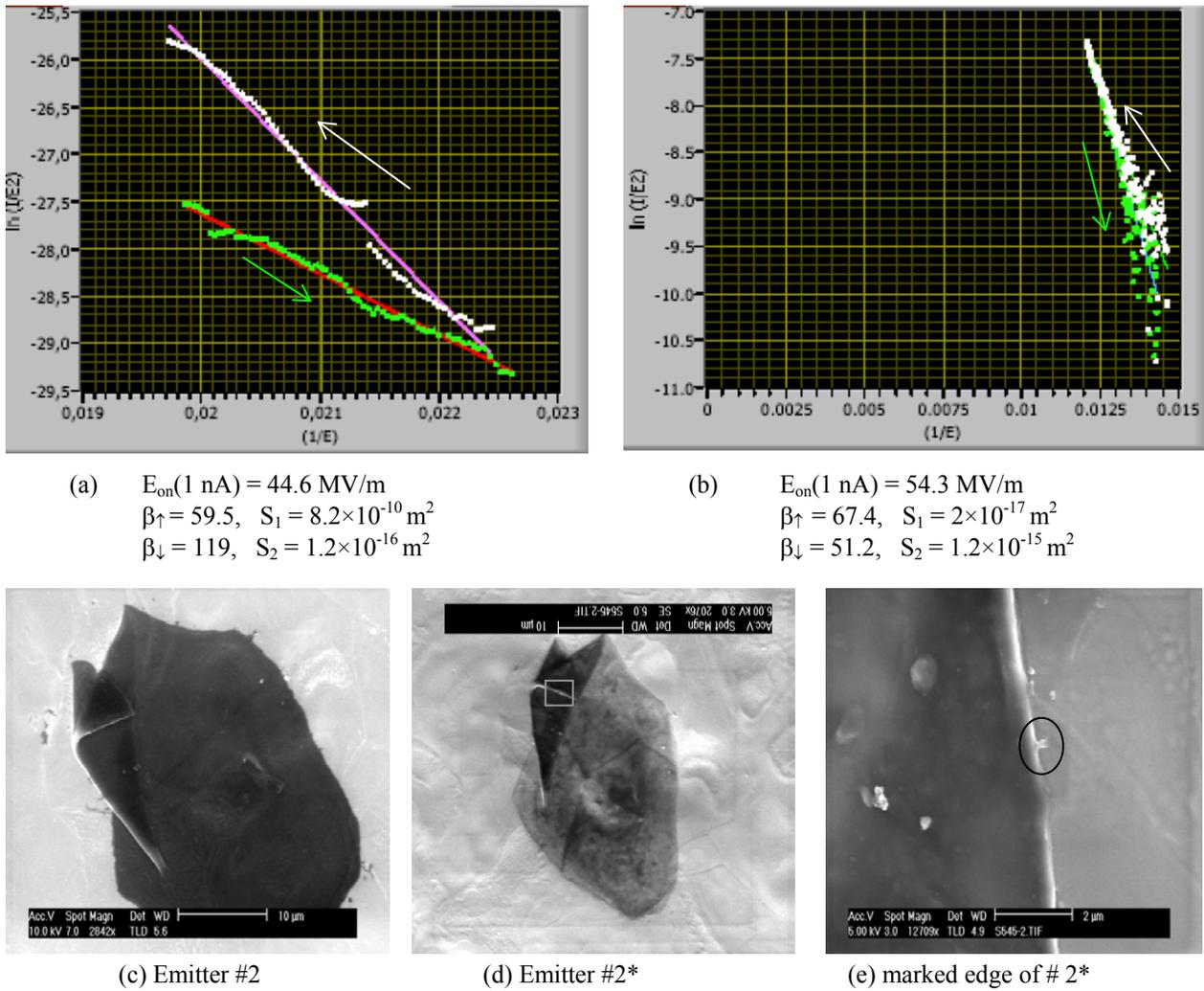
Fig.5:　FN curves and HRSEM images of the same emitter before (#2) and after HPR (#2*).

Since HPR is regularly used for the surface preparation of Nb cavities, we have tried to identify all emitters found in Fig. 1(l) by SEM. While no obvious feature was found in the area of emitter #1*, pronounced objects appeared in the SEM images for emitters #3* and #4*. Fig. 6(left) shows a scratch-like surface irregularity of about 100 µm length with terraced edges probably caused by a massive tool, but EDX analysis revealed only Nb there. Therefore, strong but very local geometric field enhancement can be expected which fits to the high β and low S value of emitter #3*. In contrast Fig. 6(middle) shows a crystalline particle of some ten µm size with some edges, which fit well to the measured β and S values of emitter #4*. This particle partially consists of S, Cl and K as revealed by the EDX spectrum in Fig. 6(right). Considering the large size of all identified objects, the EFE of Nb should be reducible by improved surface preparation techniques.
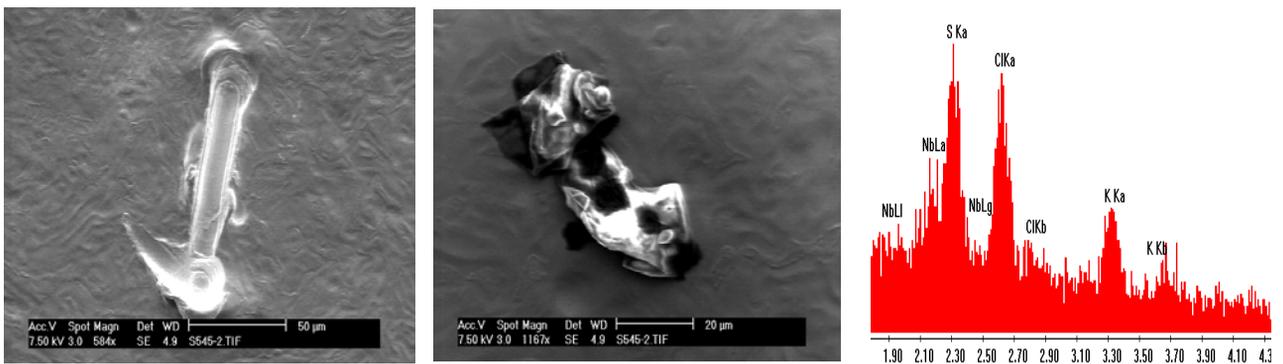
Fig. 6:　SEM images of emitter #3* (left) and #4* (middle). The EDX spectrum of #4* (right) shows S, Cl, K contents.

4. CONCLUSIONS

Systematic FE scans of EP Nb samples have given onset fields of 40-60 MV/m and emitter number densities up to $30/cm^2$ at 120 MV/m which were about halved after HPR. Since some of the emitters might have been welded on the surface by the FE current, further reduction is expected for EP samples directly cleaned by HPR. The strongest of these emitters were localized on a μm scale. Most of them showed stable FN-like I-V curves with β values of 31 to 231 and S-parameters of 10^{-12} to 10^{-20} m^2 which are typical for particulates and surface irregularities on Nb. Some emitters were identified by high resolution SEM and EDX investigations. The only HPR resistent emitter turned out to be a thin conductive object with a folded edge and submicron protrusions, which mainly consists of Nb. Moreover, a scratch-like surface defect and a crystalline particle with S, Cl and K content were found as emitters after HPR. The rather large size and nature of these identified objects gives hope to avoid FE in Nb cavities by improved surface preparation techniques up to the fields required for XFEL and ILC.

ACKNOWLDGEMENT

REFERENCES

[1] TESLA XFEL Technical Design Report Supplement, eds. R. Brinkmann et al., DESY 2002-167 (2002) and K. Floettmann, Proc. of this workshop.

[2] I.V. Bazarov, H. Padamsee, TESLA Report 2005-09 and Proc. of this workshop (2005).

[3] E. Mahner, N. Minatti, H. Piel, N. Pupter, Appl. Surf. Sci. 67, 23 (1993).

[4] D. Lysenkov, G. Müller, Int. J. Nanotechnology, special issue "Nanotechnology toolkit", Sept. (2005).

[5] D. Reschke, A. Brinkmann, D. Werner, G. Müller, Proc. Lin. Acc. Conf., Lübeck 2004.

[6] T. Habermann, Thesis, University of Wuppertal, WUB-DIS 98-18 (1999).

[7] T. Habermann, A. Göhl, D. Nau, G. Müller, H. Piel, M. Wedel, Part. Acc. 61, 137 (1998).

[8] M. Jimenez , R.J. Noer, G. Gouve, J. Jodet, B. Bonin, J. Phys. D: Appl. Phys. 27, 1038 (1994).

[9] J. Knobloch, H. Padamsee, Part. Acc. 61, 169 (1998).